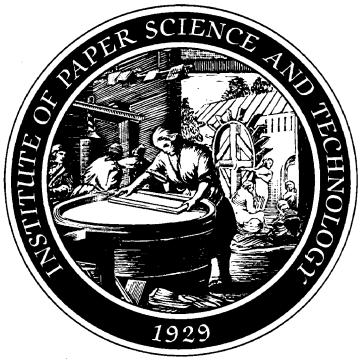

Institute of Paper Science and Technology
Atlanta, Georgia

IPST Technical Paper Series Number 624

On the Elasticity of Isotropic Fiber Systems

M. Ostoja-Starzewski

September 1996

Submitted to
Journal of Pulp and Paper Science

INSTITUTE OF PAPER SCIENCE AND TECHNOLOGY
PURPOSE AND MISSIONS

The Institute of Paper Science and Technology is a unique organization whose charitable, educational, and scientific purpose evolves from the singular relationship between the Institute and the pulp and paper industry which has existed since 1929. The purpose of the Institute is fulfilled through three missions, which are:

- to provide high quality students with a multidisciplinary graduate educational experience which is of the highest standard of excellence recognized by the national academic community and which enables them to perform to their maximum potential in a society with a technological base; and
- to sustain an international position of leadership in dynamic scientific research which is participated in by both students and faculty and which is focused on areas of significance to the pulp and paper industry; and
- to contribute to the economic and technical well-being of the nation through innovative educational, informational, and technical services.

ACCREDITATION

The Institute of Paper Science and Technology is accredited by the Commission on Colleges of the Southern Association of Colleges and Schools to award the Master of Science and Doctor of Philosophy degrees.

NOTICE AND DISCLAIMER

The Institute of Paper Science and Technology (IPST) has provided a high standard of professional service and has put forth its best efforts within the time and funds available for this project. The information and conclusions are advisory and are intended only for internal use by any company who may receive this report. Each company must decide for itself the best approach to solving any problems it may have and how, or whether, this reported information should be considered in its approach.

IPST does not recommend particular products, procedures, materials, or service. These are included only in the interest of completeness within a laboratory context and budgetary constraint. Actual products, procedures, materials, and services used may differ and are peculiar to the operations of each company.

In no event shall IPST or its employees and agents have any obligation or liability for damages including, but not limited to, consequential damages arising out of or in connection with any company's use of or inability to use the reported information. IPST provides no warranty or guaranty of results.

ON THE ELASTICITY OF ISOTROPIC FIBER SYSTEMS

Martin Ostoja-Starzewski
Institute of Paper Science and Technology
500 10th St., N.W.
Atlanta, GA 30318-5794, U.S.A.

ABSTRACT

Of concern is a micromechanical derivation of effective stiffnesses of paper from fiber properties. Special attention is given to the problem of a mechanical model of interacting fibers - either fibers carrying axial forces or fibers carrying axial, shear, and bending forces. The choice of such a discrete model, set in the context of a triangular lattice, is closely related to the type of a continuum approximation: either classical or micropolar. It is found that, as the fiber density grows, the fiber bending tends to increase the effective Young's modulus and decrease the effective Poisson's ratio. A full comparison with the theory of Cox requires an introduction of a perforated plate model for the regime of high fiber density.

INRODUCTION

One of the fundamental challenges in paper physics is the determination of effective continuum-type elastic properties from the fiber mechanics and fiber-fiber interactions. Considering the composite material structure of every single fiber, one is naturally tempted to replace it by an appropriate mechanical element and proceed to derive the overall properties of a system of fibers that makes up the paper sheet. Such was the approach originated by Cox [1], whereby the fibers were taken as axial load carrying elements. However, the simple observation that fiber-fiber contacts are of a finite surface area, suggests that they act as 'welded' contacts, so that fibers must really behave as flexing beams. Examination of the effect of this flexing on the effective in-plane elastic moduli of paper is one of the goals of the present study, with attention being focused on the isotropic case - handsheets.

Let us note another aspect of the Cox model: an assumption of straight fibers that span the entire domain of the paper sheet under consideration. This justified the state of uniform strain, whereby the effective stiffnesses could be derived. Additionally, the domain over which an integration with respect to an angular distribution function of fiber orientations was carried out, played the role of a Representative Volume Element (RVE). Now, in the case of finite length fibers - i.e., shorter than the RVE dimensions - the uniform strain assumption is not correct unless one deals with a unit cell of a regular lattice of fibers, and in that case, the unit cell becomes an RVE. We are thus led to a triangular lattice model, whose advantage lies in a possibility of explicitly deriving the effective moduli in terms of the fiber stiffnesses and fiber volume fraction in the sheet. In order to assess the basic types of possible dependencies, the analysis is set in the context of an isotropic in-plane response that corresponds to handsheets.

The first system we consider is a regular triangular lattice of elements (fiber segments) carrying axial forces only. This model is then generalized to the case of elements behaving as extensible, flexing beams; these two lattice models have their roots in the crystal lattice theory. As the porosity decreases, this treatment of fiber segments as beams becomes questionable, and a porous plate model is introduced. Throughout the paper, comparisons of these models to the Cox model are being made, with the final conclusions drawn in the last section.

POROSITY IN A LATTICE MODEL

It will be important, for the sake of reference, to have several basic relationships [2]. First,

grammage is defined as

$$W \equiv \frac{m}{L \times L} \tag{1}$$

where m is the total mass of fibers in the given $L \times L$ window and is given as $m = V_f \rho_f = V \rho_a$. Here V_f is the total volume occupied by all the fibers; ρ_f is the mass density of the fibers; $V = L^2 t_a$ is the total volume; and ρ_a is the apparent mass density; and t_a is the apparent thickness. Next, the fiber volume fraction and the porosity (or the volume fraction of pores) are

$$P_f \equiv \frac{V_f}{V} \qquad P_p \equiv \frac{V - V_f}{V} = 1 - P_f = 1 - \frac{\rho_a}{\rho_f} \tag{2}$$

Notations P_f and P_p reflect the fact that these are the probabilities of hitting the f-phase (fibers) or the p-phase (pores) in an image analysis.

There are, basically, three periodic nearest-neighbor lattices in two dimensions (2D): triangular, square, and honeycomb. Now, a square lattice would result in an orthotrpic response, while a honeycomb lattice would seem too remote from any fiber microstructure. Thus, given our interest in isotropic materials, we take a triangular lattice (Fig. 1a) as an idealized model of a single-layer fiber network, which may be interpreted as a single-layer mat of intersecting long fibers. The internode elements play the role of free fiber segments [2]; their thickness, width, and length are denoted by t_a, w, and the internode spacing s, respectively. Pores are clearly defined in such a lattice (Fig. 1b), so that porosity P_p and relative bonded area RBA are expressed in terms of the fiber aspect ratio w/s

$$P_f = 2\sqrt{3}\frac{w}{s} - 3\left(\frac{w}{s}\right)^2 \qquad RBA = \frac{2\frac{w}{s}}{2\sqrt{3} - 3\frac{w}{s}} \tag{3}$$

Note that in the hypothetical limiting case of $P_f = 1.0$, $w/s = 1/(\sqrt{3})$, and RBA becomes 2/3. On the other hand, in the case of $P_f = 0.0$, $w/s = 0$, and $RBA = 0$. In the following, a formula, inverse to (3), will be useful

$$\frac{w}{s} = \frac{1 - \sqrt{1 - P_f}}{\sqrt{3}} \tag{4}$$

Considering the fiber overlap at the lattice nodes of either lattice, one could proceed here with a somewhat different interpretation for the apparent thickness of the fiber mat: namely, t_a to be

effectively equal to three or two fiber thicknesses rather than just one. The ambiguity of t_a for 2D fiber mats is also noted in other models of fiber networks. For example, Kallmes & Corte [3] define a 2D sheet as one in which the area covered by more than two fibers is negligible, i.e., less than 1%.

TWO-DIMENSIONAL (PLANAR) VERSUS THREE-DIMENSIONAL ELASTICITY

Classical Elasticity

Measurement of the z-direction strain in tensile tests of paper sheets is a challenge, e.g., [4]. Noting such experimental constraints as well as the 2D character of a generic fiber mat model, it is more convenient to work with a so-called planar rather than the conventional *3D elasticity*. This section is thus devoted to a brief exposition of basic concepts of a *planar elasticity* (or *2D elasticity*) in x_1-x_2, and its relation to the 3D elasticity.

We begin by noting that the constitutive relations for a linear elastic isotropic 3D material are

$$\varepsilon_{11} = \frac{1}{E_{3D}}[\sigma_{11} - \nu_{3D}(\sigma_{22} + \sigma_{33})] \qquad \varepsilon_{12} = \frac{1+\nu_{3D}}{E_{3D}}\sigma_{12} \tag{5}$$

together with cyclic permutations $1 \rightarrow 2 \rightarrow 3$, whereby E_{3D} and ν_{3D} stand for the conventional 3D Young's modulus and Poisson's ratio. On the other hand, in 2D elasticity, there is no x_3 direction, so that we have

$$\varepsilon_{11} = \frac{1}{E}[\sigma_{11} - \nu\sigma_{22}] \qquad \varepsilon_{12} = \frac{1+\nu}{E}\sigma_{12} \tag{6}$$

with cyclic permutation $1 \rightarrow 2$. In (6), E and ν stand for the 2D (or planar) Young's modulus and Poisson's ratio. Applying the concept of bulk and shear moduli to the above relations, we readily find that the *planar bulk and shear moduli* are

$$K = \frac{E}{2(1-\nu)} \qquad \mu = \frac{E}{2(1+\nu)} \tag{7}$$

Furthermore, the planar Young's modulus, E, and Poisson's ratio, ν, are connected to these by

$$\frac{4}{E} = \frac{1}{K} + \frac{1}{\mu} \qquad \nu = \frac{K-\mu}{K+\mu} \tag{8}$$

It is important to note here that ν is seen to range from -1 through +1, in contradistinction to ν_{3D}, which is bounded by $-1 \le \nu_{3D} \le 0.5$. For positive values of ν and ν_{3D}, we have the following

relationships

$$E = \frac{E_{3D}}{1-\nu_{3D}^2} \qquad \nu = \frac{\nu_{3D}}{1-\nu_{3D}} \tag{9}$$

We refer to [5] for a detailed discussion of relationships among this planar, the well-known plane stress, the well-known plane strain, and the 3D isotropic elasticity.

Micropolar Elasticity

It will be shown below that the presence of beam-type interactions in a fiber network necessitates a consideration of an additional degree of freedom besides two in-plane dispalcements, namely the rotation φ about an axis normal to the plane of the sheet. The force transmission now occurs not only through the surface force traction, but also through the surface moment traction. This leads to a so-called *micropolar elasticity* model, and the corresponding constitutive law is of the following form

$$\varepsilon_{11} = \frac{A+S}{4}(\sigma_{11}+\sigma_{22}) - \frac{S}{2}\sigma_{22} \qquad \varepsilon_{12} = \frac{S}{4}(\sigma_{12}+\sigma_{21}) + \frac{P}{4}(\sigma_{12}-\sigma_{21}) \qquad 1 \to 2$$
$$\kappa_1 = M\mu_1 \qquad 1 \to 2 \tag{10}$$

with cyclic permutations as shown. In the above, we use κ's to denote torsion-curvatures, while ε_{ij}'s are now asymmetric strains and σ_{ij}'s asymmetric stresses. Also, in (10), we introduced four planar compliances

$$A = \frac{1}{K} = \frac{1}{\lambda+\mu} \qquad S = \frac{1}{\mu} \qquad P = \frac{1}{\alpha} \qquad M = \frac{1}{\gamma+\varepsilon} \tag{11}$$

Observe that $(11)_1$ defines a planar bulk compliance K, and $(11)_2$ a planar shear compliance S, which is the same as the 3D shear compliance. It is noteworthy that the planar Young's modulus and Poisson's ratio are given through (8) as before; see [6] for a complete exposition of the 3D micropolar theory and [7] for a planar setting.

A LATTICE OF FIBERS CARRYING AXIAL FORCES

Consider a regular triangular lattice of Fig. 1a) with central force interactions only, that is, one where each bond represents an elastic spring (or fiber) f, all of which are connected by frictionless

nodes. Next, let us introduce hexagonal-shaped unit cells centered at each node (Fig. 1c), which are made of half-lengths of all six springs incident onto the node. It will be convenient to take the spacing s of the triangular mesh to be $2l$. Thus, the area of the hexagonal cell is $A = 2\sqrt{3}l^2$. The constitutive (force-displacement) response law of each spring is given as

$$F_i = k^{(f)} n_i^{(f)} n_j^{(f)} u_j \qquad k^{(f)} = \frac{A^{(f)} E^{(f)}}{l} \tag{12}$$

In the above,

$k^{(f)}$ is an effective (axial) spring constant of the fiber within the hexagonal cell;

$n_i^{(f)}$ is a component, in tensor notation, of a vector aligned with the fiber;

$u_j^{(f)}$ is a displacement component;

$A^{(f)} = t_a w$ is a cross-sectional area of the fiber;

$E^{(f)}$ is a Young's modulus of the fiber; and

l is a half-length of each fiber, i.e., the part contained within the hexagonal cell.

Let us now assume the cell to be under uniform strain $\bar{\underset{\sim}{\varepsilon}}$ so that the displacement field is linear

$$u_i = \bar{\varepsilon}_{ij} x_j \tag{13}$$

It follows from (13) that the strain energy of a unit hexagonal cell of such a lattice, under conditions of uniform strain $\bar{\underset{\sim}{\varepsilon}}$, is a sum of energy contributions of six fiber segments ($f = 1, \ldots, 6$)

$$U_{network} = \frac{1}{2}\bar{\varepsilon}_{ij}\bar{\varepsilon}_{km}\frac{l^2}{2}\sum_{f=1}^{6} k^{(f)} n_i^{(f)} n_j^{(f)} n_k^{(f)} n_m^{(f)} \tag{14}$$

On the other hand, the strain energy of the same unit cell, in the continuum sense, is expressed in the tensor notation by

$$U_{continuum} = \frac{A}{2}\bar{\varepsilon}_{ij} C^{eff}_{ijkm} \bar{\varepsilon}_{km} \tag{15}$$

By the energy equivalence $U_{network} = U_{continuum}$, the *effective stiffness* tensor is now calculated from (14) and (15) as

$$C^{eff}_{ijkm} = \frac{l^2}{A}\sum_{f=1}^{6} k^{(f)} n_i^{(f)} n_j^{(f)} n_k^{(f)} n_m^{(f)} \tag{16}$$

The existence of the strain energy implies a symmetry $ij \leftrightarrow km$, which reduces the number of stiffness components from 16 to 10. Next, the symmetries $i \leftrightarrow j$ and $k \leftrightarrow m$, which follow from

the definition of stress and strain tensors, reduce that total number to 6. Furthermore, the symmetries of the equialteral lattice imply $C_{1111} = C_{2222}$ and $C_{1112} = C_{2212} = 0$. And finally, by inspection of (16), the symmetry $j \leftrightarrow k$ indicates that a Cauchy relation

$$C_{1212} = C_{1122} \tag{17}$$

holds, which is expected in any system carrying axial, node-to-node forces only [8]; this will change in fiber networks carrying non-axial forces as discussed below. Thus, C^{eff}_{ijkl} will only have two independent components with Poisson's ratio 1/3. However, we should also ask a question: under what conditions is the assumption (13) correct? In other words, if we were to displace the end points of six fibers at the boundary of the hexagonal cell according to (13), under what conditions would the center point displace according to (13) as well?

Assumption of the uniform strain is correct in the special (but not the only) case of all the $k^{(f)}$ spring constants being the same, and we get from (16)

$$C^{eff}_{ijkm} = \frac{l^2 k^{(f)}}{A} \sum_{f=1}^{6} n_i^{(f)} n_j^{(f)} n_k^{(f)} n_m^{(f)} \tag{18}$$

and calculate

$$C^{eff}_{1111} = C^{eff}_{2222} = \frac{9}{8\sqrt{3}} k^{(f)} \qquad C^{eff}_{1122} = C^{eff}_{2211} = \frac{3}{8\sqrt{3}} k^{(f)} \qquad C^{eff}_{1212} = \frac{3}{8\sqrt{3}} k^{(f)} \tag{19}$$

The effective planar bulk and shear moduli, K^{eff} and μ^{eff}, are related to the $k^{(f)}$ constant by

$$K^{eff} = \frac{\sqrt{3}}{4} k^{(f)} \qquad \mu^{eff} = \frac{\sqrt{3}}{8} k^{(f)} \tag{20}$$

Recalling formula (7), we find

$$E^{eff} = E^{eff} = \frac{k^{(f)}}{\sqrt{3}} \qquad \nu^{eff} = \frac{1}{3} \tag{21}$$

Clearly, ν^{eff} does neither depend on the fiber stiffness, nor on the microstructural geometry. However, the effective Young's modulus E^{eff} does, and, in view of (11), we find

$$E^{eff} = \frac{t_a}{\sqrt{3}} \frac{w}{l} E^{(f)} \tag{22}$$

Furthermore, noting (3), we obtain

$$\frac{E^{eff}}{t_a E^{(f)}} = 2\frac{1-\sqrt{1-P_f}}{3} \tag{23}$$

The above can now be compared with the well-known formula of Cox-type theories (e.g., [1, 2]). We start with

$$E^{eff} = \frac{1}{3}\frac{W}{\rho_f}E^{(f)} \qquad \nu^{eff} = \frac{1}{3} \tag{24}$$

Thus, E^{eff} can be compared between both models in terms of porosity P_f, and in a nondimensionalized form (recall eqs. (1-2)) it is

$$\frac{E^{eff}}{t_a E^{(f)}} = \frac{P_f}{3} \tag{25}$$

It is now evident that the Cox model predicts a linear dependence on P_f, while a nonlinear dependence is seen in (23). The reason for this qualitative difference is that the Cox-type formula accounts for the fibers' density in the sheet only, but not for their geometry as expressed by the aspect ratio w/s. In other words, no length scales appear in the Cox model. A quantitative comparison of both models is given in Figs. 2a) and c). In particular, the new Young's modulus displays a nonlinearly increasing behavior as opposed to a linear behavior of the Cox model; we have the agreement of both models in the limiting case $P_f = 0$. On the other hand, both models predict the same Poisson's ratio.

A LATTICE OF FIBERS CARRYING AXIAL, SHEAR, AND BENDING FORCES

The fact that any two cellulosic fibers have a finite contact area calls into question any fiber network model in which fiber segments are joined by pinned joints. Therefore, let us now consider the regular triangular lattice of Fig. 1 again, but now with the free fiber segments (node-to-node) behaving as flexing beams and connected through 'welded contacts' at their mutual bonds. A plan view of such a single-fiber network is given in Fig. 3a), where, same as in the section on axial-force fiber model, the lattice nodes are assumed to have the same thickness as the single fiber.

In accordance with the general concepts of Fig. 3b), we have to focus on the deformations of a typical beam-fiber, its bending into a curved arch allowing the definition of its curvature, and a cut in a free body diagram specifying the normal force F, the shear force $\tilde{F}$, and the bending moment

M. It follows that the force field within the fiber network is now described by fields of force-stresses σ_{kl} and moment-stresses m_k; note the additional presence of moment-stresses due to the beam-type fiber interactions. In a continuum sense, this lattice will be approximated by the micropolar elastic medium discussed in an earlier section. While full derivation of the correspondence of such beam lattices and micropolar media has been given in [9], in the following, we give a simple account, along with an adaptation to fiber structures, of the principal results that are relevant to our problem; see also [10].

The kinematics of the fiber network are described by three functions

$$u_1(\underset{\sim}{x}) \qquad u_2(\underset{\sim}{x}) \qquad \varphi(\underset{\sim}{x}) \tag{26}$$

which coincide with the actual displacements (u_1, u_2) and rotations (φ) at the fiber-fiber intersections. Similar to (13), these functions are assumed to be linear, although the torsion-curvature $\bar{\kappa}_i$ now enters the picture in addition to the strain $\bar{\varepsilon}_{ij}$; recall $(10)_3$. As before, the overbars denote spatial averages over the unit cell. These two tensors are related to u_1, u_2, and φ by

$$\bar{\varepsilon}_{ij} = u_{j,i} + \varepsilon_{ij}\varphi \qquad \bar{\kappa}_i = \varphi_{,i} \tag{27}$$

where ε_{lk} is the 2D counterpart of the permutation tensor.

On the other hand, we note from the mechanics of beams that the response (force-displacement and moment-rotation) laws of each fiber segment are given as

$$F^{(f)} = E^{(f)}A^{(f)}\gamma^{(f)} \qquad \tilde{F}^{(f)} = \frac{12E^{(f)}I^{(f)}}{s^2}\tilde{\gamma}^{(f)} \qquad M^{(f)} = E^{(f)}I^{(f)}\kappa^{(f)} \tag{28}$$

where the new quantities are

$I^{(f)} = t_a w^3/12$ is the centroidal moment of inertia of the cross-sectional area of the fiber with respect to an axis normal to the plane of the fiber mat;

$\gamma^{(f)}$ is a fiber elongation; and

$\kappa^{(f)}$ is a fiber curvature.

Turning now to the continuum picture, the strain energy of the unit cell is expressed as

$$U_{continuum} = \frac{A}{2}\bar{\gamma}_{ij}C^{eff}_{ijkm}\bar{\gamma}_{km} + \frac{A}{2}\bar{\kappa}_i D^{eff}_{ij}\bar{\kappa}_j \tag{29}$$

from which we find

$$C^{eff}_{ijkm} = \sum_{f=1}^{6} n_i^{(f)} n_k^{(f)} \left(n_j^{(f)} n_m^{(f)} R^{(f)} + n_j^{(f)} n_m^{(f)} \tilde{R}^{(f)} \right) \qquad D^{eff}_{ij} = \sum_{f=1}^{6} n_i^{(f)} n_j^{(f)} S^{(f)} \tag{30}$$

where

$$R^{(f)} = \frac{2E^{(f)}A^{(f)}}{s^{(f)}\sqrt{3}} \qquad \tilde{R}^{(f)} = \frac{24E^{(f)}I^{(f)}}{\left(s^{(f)}\right)^3\sqrt{3}} \qquad S^{(f)} = \frac{2E^{(f)}I^{(f)}}{s^{(f)}\sqrt{3}} \tag{31}$$

Consistent with the assumption of rectangular fiber cross sections ($t_a \times w$), we readily establish that the ratio $\tilde{R}/R$ has a very simple significance in terms of the fiber segment's aspect ratio

$$\frac{\tilde{R}}{R} = \left(\frac{w}{s}\right)^2 \tag{32}$$

Now, if we take all the fiber segments to be the same ($R^{(f)} = R$, etc.), we find

$$\begin{gathered} C^{eff}_{1111} = C^{eff}_{2222} = \frac{3}{8}(3R+\tilde{R}) \qquad C^{eff}_{1212} = \frac{3}{8}(R+3\tilde{R}) \\ C^{eff}_{1122} = C^{eff}_{2211} = \frac{3}{8}(R-\tilde{R}) \qquad C^{eff}_{1221} = C^{eff}_{2112} = \frac{3}{8}(R-\tilde{R}) \\ D^{eff}_{11} = D^{eff}_{22} = \frac{3}{2}S \end{gathered} \tag{33}$$

with all the other components of both stiffness tensors being zero. In other words, we have

$$C^{eff}_{ijkm} = \delta_{ij}\delta_{km}\Xi + \delta_{ik}\delta_{jm}\Lambda + \delta_{im}\delta_{jk}\Pi \qquad D^{eff}_{ij} = \delta_{ij}\Gamma \tag{34}$$

in which

$$\Xi = \Pi = \frac{3}{8}(R-\tilde{R}) \qquad \Lambda = \frac{3}{8}(R+3\tilde{R}) \qquad \Gamma = \frac{3}{2}S \tag{35}$$

Note that the Cauchy relation (17) does not hold here.

The effective bulk and shear moduli are now identified as

$$K^{eff} = \frac{3}{4}R \qquad \mu^{eff} = \frac{3}{8}(R+\tilde{R}) \tag{36}$$

which are seen to reduce to the formulas (20) in the special case of flexural rigidity being absent. Furthermore, it follows that the effective Young's modulus and Poisson's ratio are

$$E^{eff} = 3R\frac{1+\frac{\tilde{R}}{R}}{3+\frac{\tilde{R}}{R}} \qquad \nu^{eff} = \frac{1-\frac{\tilde{R}}{R}}{3+\frac{\tilde{R}}{R}} \tag{37}$$

Again, let us note that these reduce to (21) in the case of fibers carrying axial forces only ($\tilde{R} = 0$). Regarding the Poisson's ratio, we observe that the introduction of beam-type effects (i.e., as $\tilde{R}/R$

increases) has a tendency to reduce it. Furthermore, noting (32), the effective Young's modulus (normalized by $E^{(f)}$ and t_a) and Poisson's ratio may be expressed in terms of the fiber aspect ratio

$$\frac{E^{eff}}{t_a E^{(f)}} = 2\sqrt{3}\frac{w}{s}\frac{1+\left(\frac{w}{s}\right)^2}{3+\left(\frac{w}{s}\right)^2} \qquad \nu^{eff} = \frac{1-\left(\frac{w}{s}\right)^2}{3+\left(\frac{w}{s}\right)^2} \tag{38}$$

or, given (4), in terms of the porosity

$$\frac{E^{eff}}{t_a E^{(f)}} = 2\left(1-\sqrt{1-P_f}\right)\Big]\frac{1+\frac{1}{3}\left(1-\sqrt{1-P_f}\right)^2}{3+\frac{1}{3}\left(1-\sqrt{1-P_f}\right)^2} \qquad \nu^{eff} = \frac{3-\left(1-\sqrt{1-P_f}\right)^2}{9+\left(1-\sqrt{1-P_f}\right)^2} \tag{39}$$

Formulas (39) have been investigated numerically in Figs. 2a) and c). First, we observe that the beam model leads to a gradual increase of E^{eff} as compared to the previous model. This may easily be explained by noting that more energy may be stored in fibers which carry shear and bending forces than in the fibers which carry axial forces only. This effect is accompanied by the Poisson's ratio falling off nonlinearly from 1/3 with P_f increasing. It is gratifying to recall the same result established in [11]: Poisson's ratio tends to decrease with the bonding of the sheet. Summarizing, the beam effects have a rather small influence on the effective isotropic elasticity.

A PERFORATED PLATE MODEL

As P_f goes beyond 50%, the aspect ratio w/s increases, and one can no longer consider the connections between the lattice nodes to be beams. Given the highly anisotropic nature of fibers and a complex composite structure of fiber systems, a basic question arises: can any simple explicit model be derived for this low porosity range? Probably not, and this problem is reflected in, for example, a recent paper series [12, 13, 14], which had to culminate in a numerical solution of a somewhat hypothetical equivalent unit cell. Another avenue is offered by brute force solutions of complex fiber systems as exemplified by [15]. Here, for the sake of completeness of our analysis, we consider the limiting case of a beam model - namely, a perforated plate.

In the limit of $P_f \to 1$, we have a plate with a regular distribution of triangular-shaped pores, Fig. 2b). This is a so-called "dilute limit" of a locally isotropic material with holes (in either periodic or disordered arrangements), that has already been solved in [16, 17]. The respective formulas are

$$\frac{E^{eff}}{t_a E^{(f)}} = 1-\alpha(1-P_f) \qquad \nu^{eff} = \nu^{(f)} - \alpha\left(\nu^{(f)} - \nu_0\right)(1-P_f) \tag{40}$$

The coefficients $\alpha = 4.2019$ and $\nu_0 = 0.2312$ have been computed in the above references, and, in fact, analogous coefficients are also available there for plates with other than triangular holes. It is noteworthy that:

i) both formulas are uncoupled from one another;

ii) the formula $(40)_1$ gives a correctly expected behavior in Fig. 2a) for very high values of P_f, in place of the beam lattice model;

iii) the formula for ν^{eff} depends on the Poisson's ratio $\nu^{(f)}$ of the plate material, a value which cannot be specified since the fibers are strongly anisotropic; we therefore do not plot ν^{eff} for this model.

One more question remains with reference to Fig. 2b): what happens in the range of the P_f values which are too high for a beam lattice model to hold and too low for the dilute model to be truly dilute? Or, in terms of Fig. 2a), can anything be done to smooth out the transition between the two curves 3 and 4 at P_f around 0.8 ? Let us try here a usual device of micromechanics: an effective medium theory. Following [16, 17], we adopt a so-called 'differential scheme' which is given by

$$\frac{E^{eff}}{t_a E^{(f)}} = P_f^{\alpha} \qquad \nu^{eff} = P_f^{\alpha}\left(\nu^{(f)} - \nu_0\right) + \nu_0 \tag{41}$$

While $(41)_1$ through the curve 5 gives the desired behavior, $(41)_2$ cannot be employed for the same reason as listed in point iii) above. Summarizing, E^{eff} is modeled by an upper envelope of all the curves in Fig. 2a) - i.e., curves 3 and 5.

CONCLUSIONS

This paper presents an exploratory study of the adaptation of spring lattices to modeling elasticity of paper, that was first reported in [18]. We started with the simplest, periodic geometries that permitted an explicit derivation of effective properties based on the unit cell concept. Following are the main observations:

i) Triangular networks with axial interactions result in the Young's modulus and Poisson's ratio very similar to those obtained in Cox-type theories.

ii) Presence of the bending fiber action in addition to the axial one has the effect of increasing

the Young's modulus and of decreasing the Poisson's ratio down from 1/3. Guided by [19, 20] we expect that these effects are being countered by the spatial randomness of fibrous systems; these two studies, set in the context of random triangular lattices carrying axial forces, established that the geometric disorder decreases E^{eff} but increases ν^{eff}.

iii) The beam lattice as well as the axial lattice models can be generalized to deal with random geometries of fiber arrangements, shapes, sizes, and physical properties. Indeed, this appears to be the current trend in studies of elasticity, strength, and transport phenomena in paper. However, no close-form formulas can then be derived, and this is where the periodic models may serve as a guidance, while various types of microstructural disorder can be investigated quantitatively.

iv) In the case of high fiber density (from 50 to 100%), the beam lattice model may be replaced by a perforated plate model, which gives the theoretically correct, although physically unattainable, limiting behavior of the Young's modulus. This model is introduced here for the sake of completeness of the study.

v) Given the orthotropic character of paper sheets, lattice models can be generalized to anisotropy, both in 2D and in 3D (also modeling the multilayered paper structure).

vi) A very similar approach - lattices and perforated plates - can also be adapted to conductivity problems in fibrous systems.

REFERENCES

1. Cox, H.L., "The elasticity and strength of paper and other fibrous materials," *Brit. J. Appl. Phys.* 3: 72-79, (1952).

2. Bristow, J.A. and Kolseth, P., *Paper: Structure and Properties*, Marcel Dekker, New York, 1986.

3. Kallmes, O.J. and Corte, H., "The structure of paper - I. The statistical geometry of an ideal two dimensional fiber network," *Tappi J.* 43: 737-752 (1960).

4. Mark, R.E. and Murakami, K., *Handbook of Physical and Mechanical Testing of Paper and Paperboard*, Marcel Dekker, New York (1983).

5. Thorpe, M.F. and Jasiuk, I., "New results in the theory of elasticity for two-dimensional composites," *Proc. Roy. Soc. Lond.* A438: 531-544 (1992).

6. Nowacki, W., *Theory of asymmetric elasticity*, Pergamon Press/Polish Sci. Publ., Oxford/ Warsaw (1986).

7. Ostoja-Starzewski, M. and Jasiuk, I., "Stress invariance in planar Cosserat elasticity," *Proc. Roy. Soc. Lond.* A451: 453-470 (1995).

8. Love, A.E.H., *A Treatise on the Mathematical Theory of Elasticity*, Cambridge University Press, Cambridge (1934).

9. Wozniak, C., *Surface Lattice Structures* (in Polish), Polish Sci. Publ., Warsaw (1970).

10. Ostoja-Starzewski, M, Sheng, P.Y., and Alzebdeh, K., "Spring network models in elasticity and fracture of composites and polycrystals," *Computational Materials Science*, in press (1996).

11. Schulgasser, K. and Page, D., "The influence of transverse fibre properties on the in-plane elastic behaviour of paper," *Composites Science and Technology* 32: 279-292 (1988).

12. Lu, W., Carlsson, L.A., and Andersson, Y., "Micro-model of paper. Part I: Bounds on elastic properties," *Tappi J.* 78(12): 155-164 (1995).

13. Lu, W. and Carlsson, L.A., "Micro-model of paper. Part II: Statistical analysis of the paper structure," *Tappi J.* 79(1): 155-210 (1996).

14. Lu, W. and Carlsson, L.A., "Micro-model of paper. Part III: Mosaic model," *Tappi J.* 79(2): 197-205 (1996).

15. Jangmalm, A. and Östlund, S., "Modelling of curled fibers in two-dimensional networks," *Nordic Pulp Pap. Res. J.* 3: 156-161 (1995).

16. Jasiuk, I., Chen, J., and Thorpe, M.F., "Elastic moduli of two dimensional materials with polygonal holes," *Applied Mechanics Reviews* 47(1, Part 2): S18-S28 (1994).

17. Jasiuk, I., "Polygonal cavities vis-à-vis rigid inclusions: Effective elastic moduli of materials with polygonal inclusions," *International Journal of Solids and Structures* 32: 407-422 (1995).

18. Ostoja-Starzewski, M., "Random fiber networks: Bounds on effective elastic and transport moduli," *1996 Progress in Paper Physics - A Seminar*, Stockholm.

19. Ostoja-Starzewski, M. and Wang, C., "Linear elasticity of planar Delaunay networks: Random field characterization of effective moduli," *Acta Mech.* 80: 61-80 (1989).

20. Ostoja-Starzewski, M. and Wang, C., "Linear elasticity of planar Delaunay networks. II: Voigt and Reuss bounds, and modification for centroids," *Acta Mech.* 84: 47-61 (1990).

Figure Legends

Fig. 1a) A triangular lattice with a hexagonal unit cell shown; b) pore structure in a triangular lattice network; c) six fiber segments ($f = 1, 2, \ldots, 6$) in a single hexagonal cell, showing the numbering of six springs $k^{(f)}$.

Fig. 2a) Effective Young's moduli as a function of the fiber density P_f for the Cox model (1), the axial-fibers lattice (2), the beam-fibers lattice (3), the dilute limit of a perforated plate (4), and the effective medium for a perforated plate (5); b) the corresponding decrease in pore dimensions - from slender beams to small holes at P_f = 10%, 50%, and 90%; c) effective Poisson's ratios as a function of the fiber density P_f for the Cox model (1), the axial-fibers lattice (2), and the beam-fibers lattice (3).

Fig. 3a) A plan view of a triangular lattice of beam-type fibers; b) internal loads in a fiber; c) curvature of a deformed fiber.

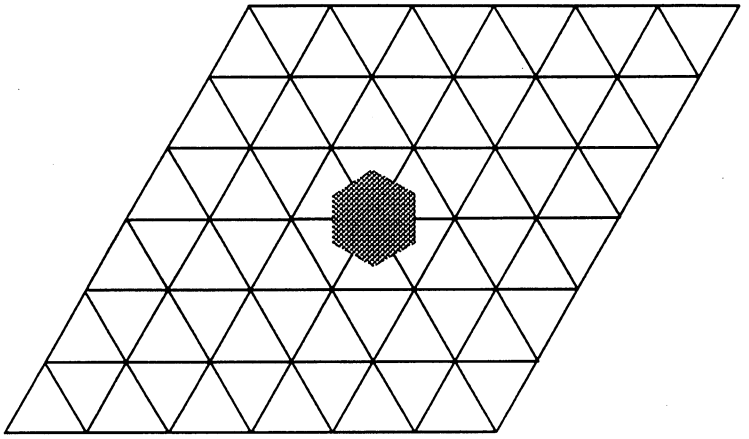

a)

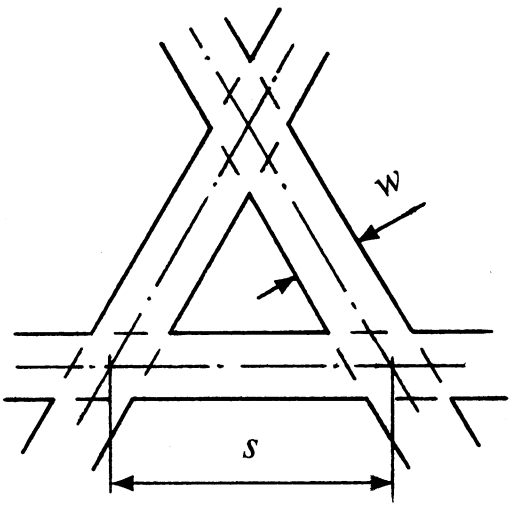

b)

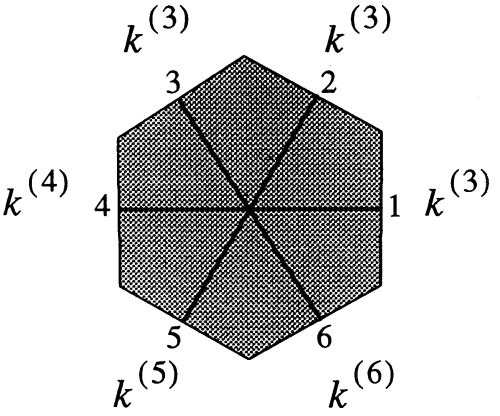

c)

Fig. 1

a)

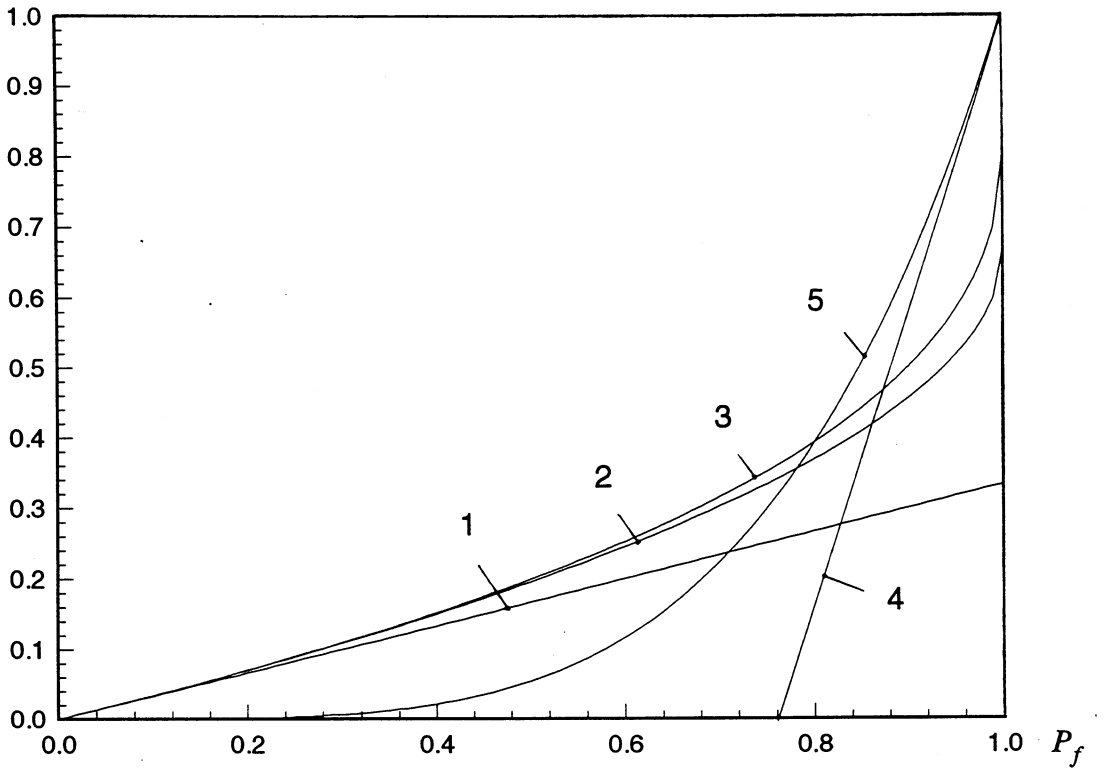
1.0
0.9
0.8
0.7
0.6
0.5
0.4
0.3
0.2
0.1
0.0
0.0
0.2
0.4
0.6
0.8
1.0
P_f
1
2
3
4
5

b)

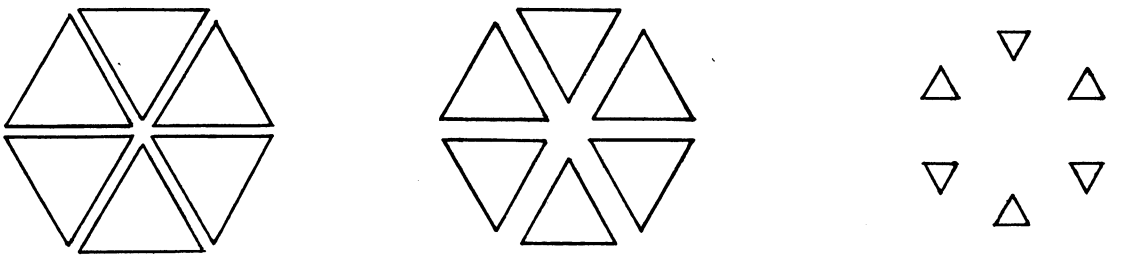

c)

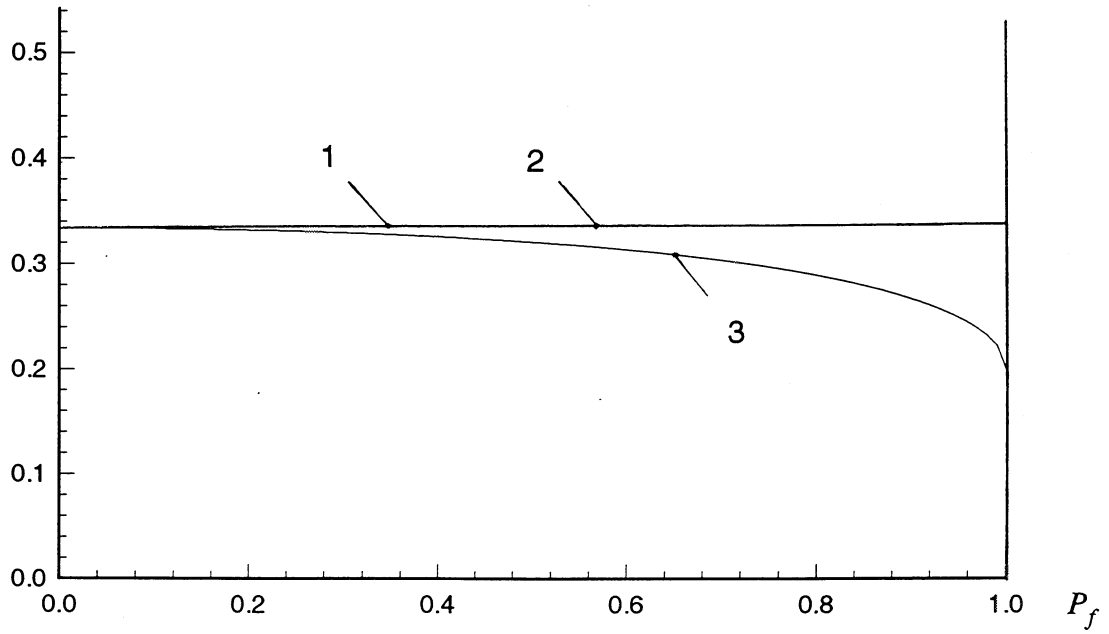
0.5
0.4
0.3
0.2
0.1
0.0
0.0
0.2
0.4
0.6
0.8
1.0
P_f
1
2
3

Fig. 2

a)

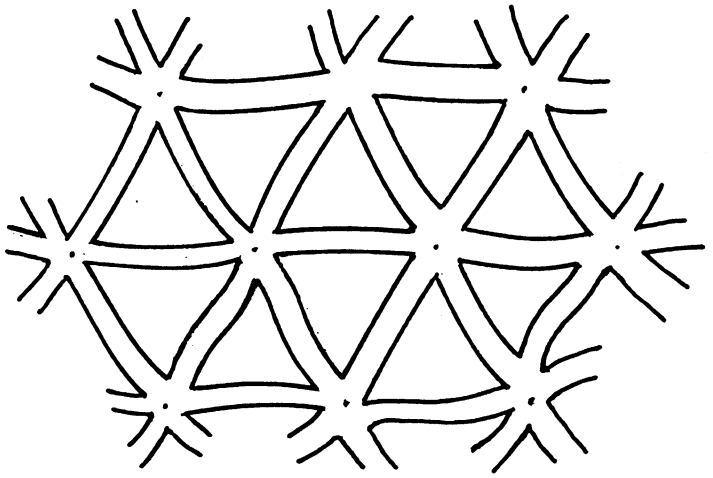

b)

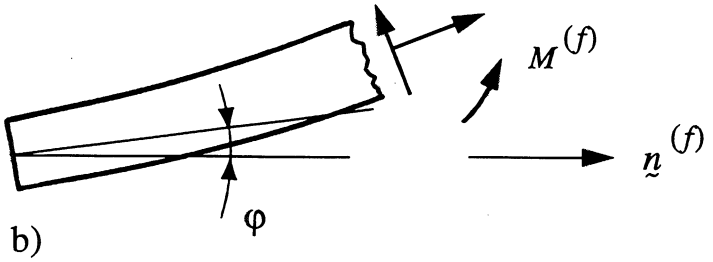

c)

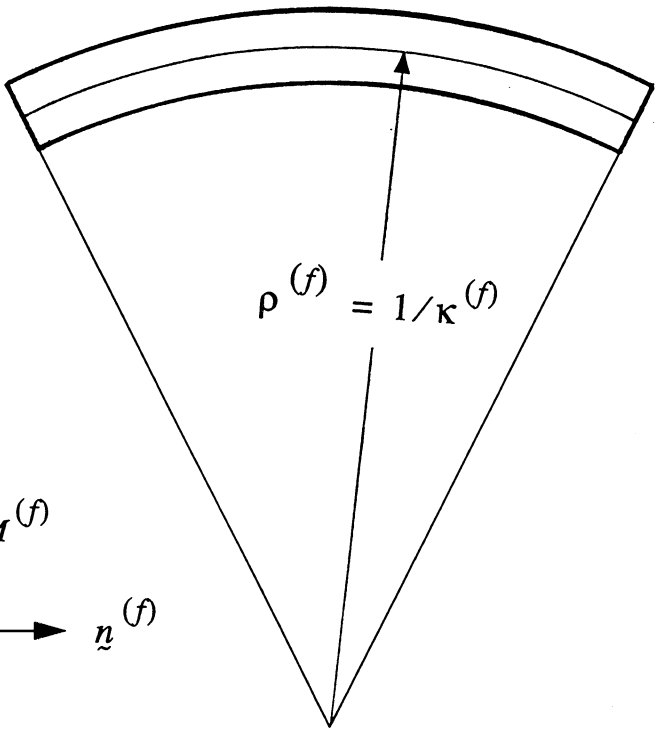

Fig. 3